Title

Investigating Microtopographic and Soil Controls on a Mountainous Meadow Plant Community Using High-Resolution Remote Sensing and Surface Geophysical Data

Journal

Journal of Geophysical Research: Biogeosciences, 124(6)

ISSN

2169-8953

Authors

Falco, N
Wainwright, H
Dafflon, B
et al.

Publication Date

2019-06-01

DOI

10.1029/2018JG004394

Peer reviewed

Investigating Microtopographic and Soil Controls on a Mountainous Meadow Plant Community Using High-Resolution Remote Sensing and Surface Geophysical Data

Nicola Falco[1], Haruko Wainwright[1], Baptiste Dafflon[1], Emmanuel Léger[1], John Peterson[1], Heidi Steltzer[2], Chelsea Wilmer[2], Joel C. Rowland[3], Kenneth H. Williams[1], and Susan S. Hubbard[1]

[1] Earth and Environmental Science Area, Lawrence Berkeley National Laboratory, Berkeley, CA, USA, [2] Department of Biology, Fort Lewis College, Durango, CO, USA, [3] Earth and Environmental Sciences Division, Los Alamos National Laboratory, Los Alamos, NM, USA

Correspondence to: N. Falco, nicolafalco@lbl.gov

Abstract

This study aims to investigate the microtopographic controls that dictate the heterogeneity of plant communities in a mountainous floodplain-hillslope system, using remote sensing and surface geophysical techniques. Working within a lower montane floodplain-hillslope study site (750 m × 750 m) in the Upper Colorado River Basin, we developed a new data fusion framework, based on machine learning and feature engineering, that exploits remote sensing optical and light detection and ranging (LiDAR) data to estimate the distribution of key plant meadow communities at submeter resolution. We collected surface electrical resistivity tomography data to explore the variability in soil properties along a floodplain-hillslope transect at 0.50-m resolution and extracted LiDAR-derived metrics to model the rapid change in microtopography. We then investigated the covariability among the estimated plant community distributions, soil information, and topographic metrics. Results show that our framework estimated the distribution of nine plant communities with higher accuracy (87% versus 80% overall; 85% versus 60% for shrubs) compared to conventional classification approaches. Analysis of the covariabilities reveals a strong correlation between plant community distribution, soil electric conductivity, and slope, indicating that soil moisture is a primary control on heterogeneous spatial distribution. At the same time, microtopography plays an important role in creating particular ecosystem niches for some of the communities. Such relationships could be exploited to provide information about the spatial variability of soil properties. This highly transferable framework can be employed within long-term monitoring to capture community-specific physiological responses to perturbations, offering the possibility of bridging local plot-scale observations with large landscape monitoring.

Plain Language Summary

In this study, we aim to understand how soil and topographic properties influence the spatial distribution of plant communities within a floodplain-hillslope system, located in a mountainous East River watershed in Colorado.

Watersheds are vulnerable to environmental change, including earlier snowmelt, changes in precipitation, and temperature trends, all of which can alter plant communities and associated water and nutrient cycles within the watershed. However, tractable yet accurate quantification of plant communities is challenging to do at a scale that also permits investigations of the key controls on the distribution. Here we developed a framework that uses a new approach to estimate plant distributions, one which exploits both remote sensing (satellite) images and surface geophysical data. Joint consideration of the aboveground-and-belowground data sets allows us to characterize both plant and soil properties at high spatial resolution and to identify the main environmental controls for plant distribution. In our analysis, we found that soil moisture and microtopography characteristics influence how plant communities are spatially distributed. Considering that each community responds to external perturbation in a different way, this method can be used within a multitemporal framework to characterize, temporally, the environmental heterogeneity at local scale and capture plant responses caused by climate-related perturbations.

1 Introduction

Mountainous watersheds are critical for water resources and essential to both ecosystems and human activities (Rangwala et al., 2013; Viviroli et al., 2007). High-elevation regions are known to be more vulnerable to climate change, particularly owing to amplified temperature increases compared to lower elevation regions (Mountain Research Initiative EDW Working Group, 2015; Wang et al., 2014). Studies have shown that a rise in temperature decreases the amount of snow-water equivalent and changes the timing of snowmelt (Ernakovich et al., 2014), both of which have a dramatic effect on ecosystem functioning, including plant phenology, community distribution, and primary productivity (Harte et al., 1995; Ohmura, 2012; Sloat et al., 2015). Changes in vegetation in turn influence both watershed water budgets (due to their substantial influence on evapotranspiration—Maxwell & Condon, 2016) and nutrient cycling (Hinckley et al., 2014; Hobbie, 2015).

In the Rocky Mountain regions of the United States where the ecosystem is often water limited, observations have detected changes in the species abundance of mountainous meadow plant communities, with shrubs in particular becoming more dominant (Spasojevic et al., 2013). Long-term plot-scale studies have shown that early snowmelt—both naturally occurring and artificially induced—has led to the shifts from forbs to woody species (Harte et al., 1995, 2015). In the same region, modeling studies have predicted that the changes in plant species from grassland to shrubland will amplify streamflow reduction as a result of the warming climate and early snowmelt (Pribulick et al., 2016). The challenge is that it is often difficult to upscale findings obtained from localized plot-scale studies to the watershed and/or regional scale. This scaling difficulty arises from the complex terrain and extreme heterogeneity that are often typical in mountainous regions.

To gain a predictive understanding of how the plant community will respond to climate change over space, it is important to understand key environmental factors controlling their spatial arrangement (Zimmermann & Kienast, 1999). Several research efforts have recognized a significant topographical effect—particularly the slope aspect (i.e., slope orientation; Pelletier et al., 2018)—on hydrological (Allen-Diaz, 1991; Webb et al., 2018) and pedological (Collins et al., 2004; Marston, 2010) processes. Such processes, on the other hand, have a significant impact on the local biogeochemistry activity (Amundson et al., 2015; Collins et al., 2004; Marston, 2010), leading to a heterogeneous composition of plant communities (Allen-Diaz, 1991; Zimmermann & Kienast, 1999). In these studies, the advances in optical remote sensing have allowed researchers to map vegetation traits, discriminate among plant species and functional types, and monitor ecosystem disturbances (Brown et al., 2016; Govender et al., 2009; Hame et al., 2015; Roth et al., 2015).

At the same time, improvements in geophysics have allowed researchers to capture subsurface physical and hydrological processes at high resolution over space (Binley et al., 2015; Rubin & Hubbard, 2005) and to investigate the interactions between the aboveground and belowground compartments of ecosystems. In mountainous regions, where soil salinity and soil temperature do not vary significantly at the local scale, soil electrical conductivity (soil EC) is often an indicator of the spatial variability of soil thickness, clay content, water content, or some combination of these characteristics (Binley et al., 2015; Miller et al., 2008; Rubin & Hubbard, 2005). Because of the strong influence of these characteristics on plant physiology, studies have found significant correlations between soil EC patterns and leaf area index (LAI; Rudolph et al., 2015), plant photosynthetic activity and growth (von Hebel et al., 2018), and vegetation vigor (Dafflon et al., 2017). The spatially extensive nature of geophysical data allows exploration of how soil properties vary spatially with characteristics such as plant species and dynamics.

Important but as yet unexplored in these studies is the impact of microtopography on meadow plant communities within hillslopes. Microtopography is the topographic variation on the order of submeters to several meters, which can be characterized mainly through airborne light detection and ranging (LiDAR) data. Recent studies conducted in Arctic regions—using high-resolution geophysical and remote sensing data—have revealed that microtopography could produce significant spatial heterogeneity in soil moisture and plant community distributions at several-meter or submeter scales (S. S. Hubbard et al., 2013; Dafflon et al., 2017; H. M. Wainwright et al., 2015). While the slope aspect of the hillslopes can be considered as a first-order large-scale control (Pelletier et al., 2018; Yetemen et al., 2015), the controlling factors within each hillslope have not yet to the authors' knowledge been investigated. Given that soil moisture is very

sensitive to microtopography, it could be an important factor governing the spatial organization of the ecosystem in a water-limited region.

Characterizing meadow plant communities at high-resolution is a challenge on its own, since they tend to have similar spectral signatures in optical remote sensing. Although LiDAR has been extensively used for quantifying plant structural information and for forest characterization (Dalponte et al., 2012; Gonzalez et al., 2010; Palace et al., 2015; Paris & Bruzzone, 2015; Sullivan et al., 2017), few studies have explored the joint use of optical remote sensing and LiDAR for characterizing mountainous meadow communities at a relatively high (few meters) resolution (Dirnböck et al., 2006; Hoersch et al., 2002; Nijland et al., 2015). In most of these studies, LiDAR-derived products were used as ancillary data for the identification of different habitats, even though the spectral and structural information could improve the discrimination of plant communities with similar spectral response and different structure. Moreover, the analysis of the contextual information (i.e., the correlation between adjacent pixels) is often neglected in the remote sensing-based meadow characterization studies. The use of contextual information (Benediktsson et al., 2018) is necessary to account for the spectral variability that increases owing to the high-geometrical detail, which can lead to a subsequent decrease in prediction performance. There is therefore a need to improve the information extraction from such rich data to achieve a better mapping of plant communities that share similar spectral and/or structural properties.

Recognizing the need to improve our understanding of microtopographic controls on meadow plant species distribution, this study aims to investigate the covariability among soil properties, microtopography, and plant community distributions within hillslopes. Specifically, we aim to (1) improve high-resolution mapping of meadow plant communities at submeter resolution, using a novel remote-sensing data-fusion framework; (2) characterize soil and land surface properties at similarly high resolution; and (3) use the high-resolution information to quantify the key environmental controls on the heterogeneous spatial distribution of the plant community.

We hypothesize that microtopography has a significant control over the spatial distribution of a plant community within hillslopes, because of its influence on near-surface soil hydrological and physical properties (Price, 2011). If topographic metrics are identified as key controls on plant community and soil property distributions, topography could potentially be used to easily estimate these properties over larger scales. To achieve this, first we develop a data-fusion framework based on machine learning that integrates spectral, structural, and contextual information from high-resolution optical remote sensing and LiDAR to estimate the distribution of plant communities in high resolution (0.5 m by 0.5 m). In this framework, the contextual information is modeled by spatial features that describe patterns such as shape and texture. The spatial features are computed by using a spatial feature engineering procedure that performs a multiscale image

filtering, the product of which is used as input to the machine learning algorithm. The use of the spatial information allows us to capture the spatial variability that characterizes each community and therefore to improve their discrimination (Falco et al., 2015). We then explore the relationships among the meadow plant community map, soil and land surface properties computed at a similar resolution from surface geophysics, and the LiDAR digital elevation model (DEM). This procedure allows us to evaluate the covariability among the estimated plant communities, soil bulk EC, and topographic properties—and then assess the information value of topographic properties for soil and vegetation spatial characterization.

We demonstrate our approach in a montane floodplain-hillslope system of the East River watershed in Colorado, considered to be a representative headwater catchment in the Upper Colorado River Basin (Markstrom et al., 2012). The proposed framework is expected to be useful as a tool for high-resolution characterization, providing spatially explicit information (such as species distribution) necessary to populate vegetation models (Franklin et al., 2016). The characterization of the spatial organization of plant communities becomes of critical importance when evaluating the physiology as a response to external stress, which varies in both intensity and timing for each specific community. In these terms, the framework could be potentially used within a multitemporal monitoring procedure to capture plant dynamics (i.e., phenology, diversity, and abundance) and responses to disturbances, such as early snowmelt and drought. At the same time, the framework offers the possibility of creating a bridge between plot-scale observations (at very small scale) and watershed scale monitoring, without losing the scale factor that governs aboveground and belowground processes.

2 Site and Data Description

2.1 Description of the Study Area

This study focuses on a lower montane floodplain-hillslope system located in the East River watershed, northeast of the town of Crested Butte, Colorado (38°55′N, 106°56′W; Figure 1a), as part of the Department of Energy Watershed Function Scientific Focus Area project. The Watershed Function Scientific Focus Area project (Susan S. Hubbard et al., 2018) aims to develop a predictive understanding of mountainous watershed function, its response to perturbations, and implications for downgradient water availability and water quality.

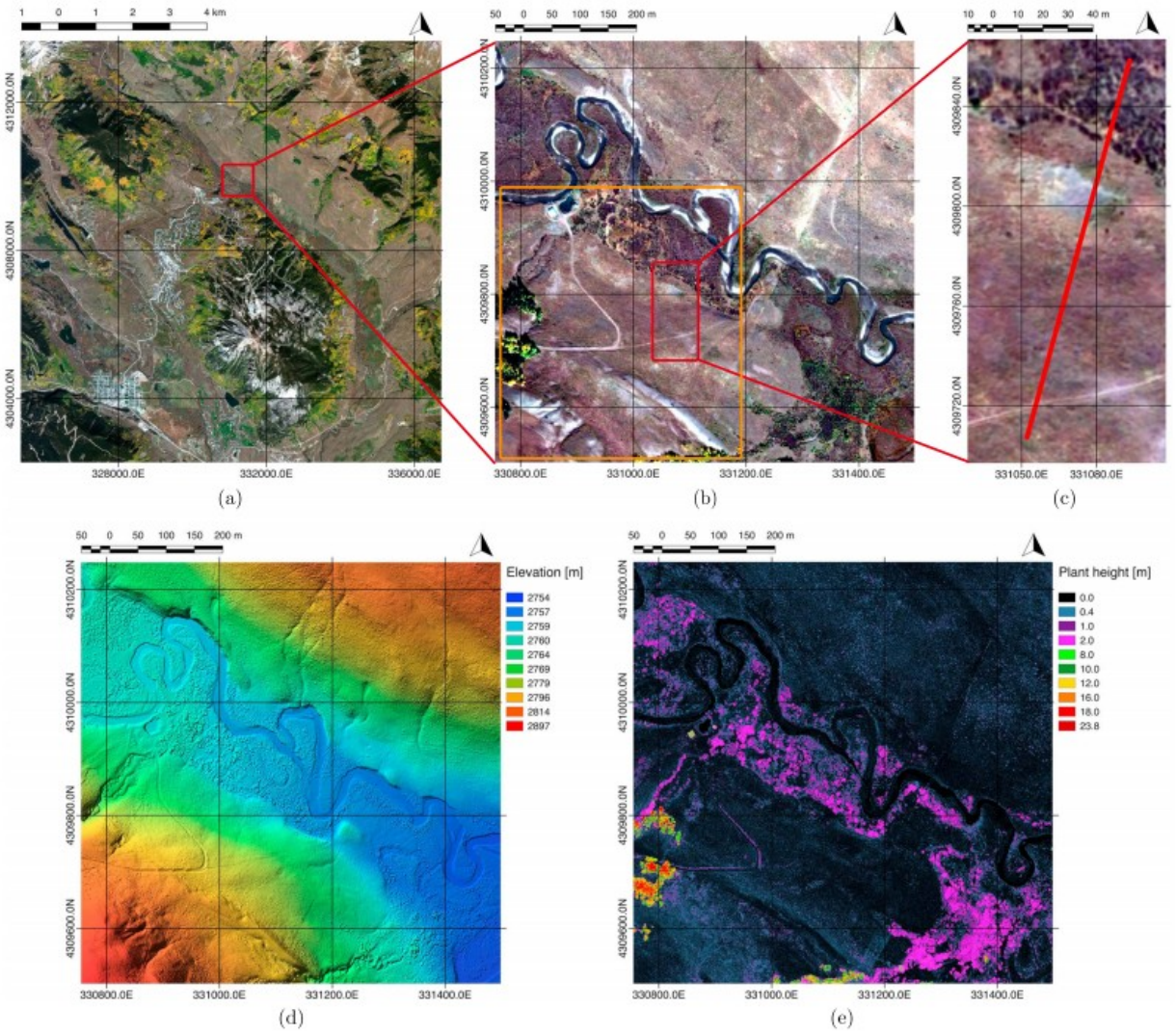

Figure 1. Area of study and remote sensing data sets: (a) WorldView-2 multispectral image (true RGB composition) of the East River watershed; (b) floodplain-hillslope study area, with the orange box indicating the extended area considered for the statistical analysis (Figure 9); (c) location of the electrical resistivity tomography transect along the hillslope gradient; (d) digital surface model obtained by the LiDAR point cloud; (e) plant height computed by subtracting the digital terrain model from the digital surface model.

The floodplain-hillslope study site (Figure 1b) is located at ~2,760-m elevation and ranges from an extensive riparian zone characterized by multiple meanders to a northeast-facing lower montane hillslope, covering a 750- × 750-m area. This site presents a diverse assortment of plant species and associated spatial distributions. The riparian zone is characterized by the presence of dwarf shrubs, such as *american dwarf birch*, *mountain willow*, and *potentilla*, divided internally by patches and narrow corridors of grassland. The floodplain-hillslope study area includes a variety of meadow plants, including *veratrum*, *frasera*, *larkspur* (*delphinium*), graminoids, dandelion, *potentialla gracilis*, *lupine*, and *sagebrush* (*artemisia*; Harte et al., 1995).

Meteorological data obtained from the SNOTEL station located in Butte (38°53′N, 106°54′W) show a high snow accumulation in fall and winter seasons (October-March), with snowmelt occurring in the spring season (April-June) and the peak of snow-water-equivalent in mid-April. The area's average temperature varies from -4.4°C in winter (December-March) to 13.5°C in summer (July-September), with average precipitation of 150.6 mm in summer and 200.8 mm in winter.

2.2 Data Collection and Preprocessing

2.2.1 Satellite Multispectral Data

An optical satellite image was acquired by the WorldView-2 (WV-2), high-resolution commercial imaging satellite operated by DigitalGlobe (Westminster, Colorado, USA) on 24 September 2015. The WV-2 system provides a panchromatic image at a spatial resolution of 0.5 m, as well as a multispectral image of eight bands at a spatial resolution of 2.0 m in the visible and the near-infrared regions (coastal, blue, green, yellow, red, red edge, NIR1, and NIR2).

Radiometric and sensor corrections were performed prior to orthorectification. In addition, we performed a pan-sharpening procedure to fuse the spectral information of the multispectral data set with the high geometrical detail of the panchromatic. We used the Gram Schmidt method (Laben & Brower, 2000) implemented in the software ENVI 5.3. Compared to several other algorithms available, this method yielded the best performance in preserving local spectral properties in this complex terrain. The geometrical resolution of the multispectral image was improved from 2 m per pixel to 0.5 m per pixel.

2.2.2 Airborne LiDAR Data

Airborne LiDAR data were acquired over the study area on 10 August 2015, using a Riegl Q1560 dual-channel LiDAR system mounted on a Piper Navajo (H. Wainwright & Williams, 2017). The survey was performed by Quantum Spatial, Inc. in collaboration with Eagle Mapping Ltd. The data comply with the U.S. Geological Survey QL1 standard (Heideman, 2014), with a point density of more than 8 pulse/m^2. From the LiDAR point cloud, we computed high-resolution DEMs: a digital surface model, representing the top-of-canopy elevation, and a digital terrain model (DTM), representing the bare-ground elevation, at the spatial resolution of 0.5 m (Figure 1d). The DEMs were compared with the real-time kinematic Global Positioning System measurements (the positioning accuracy of which is within a few centimeters) in a vegetated region within the hillslope to find that the root-mean-square error of the DEMs was less than 0.15 m.

2.2.3 In Situ Electrical Resistivity Tomography

Electrical resistivity tomography (ERT) data were acquired along a 158.75-m-long transect spanning the hillslope topographical gradient with 1.25-m

electrode spacing (Figure 1c). The transect defined by the ERT line was used to investigate the connection between the variability in soil physical properties and the diversity of plants that characterize the topographical gradient. The data were collected in October 2016 using an MPT DAS-1 electrical impedance tomography system and a dipole-dipole array configuration. The acquired resistance data served to reconstruct a 2-D model of depth-discrete soil bulk EC (or resistivity) along the transect, using a smoothness-constraint inversion code named “boundless electrical resistivity tomography” (BERT; Rücker et al., 2006a, 2006b). The obtained tomography shows a smoothed image of the soil EC spatial distribution, with a vertical resolution of roughly a third to a half of the electrode spacing near the surface. The data were resampled in a grid with cell size of a third of a meter and are reported in [S/m]. Additionally, we applied a log10 transformation to the soil EC data to decrease the skewness and facilitate the multivariate analysis. The detected range of values is between 0 and 0.03 S/m. By applying the log-transformation, the range of values results negative, with the highest negative value corresponding to the lowest soil EC. From this point forward, with soil EC we will refer to the log-transformed soil EC (Figure 2).

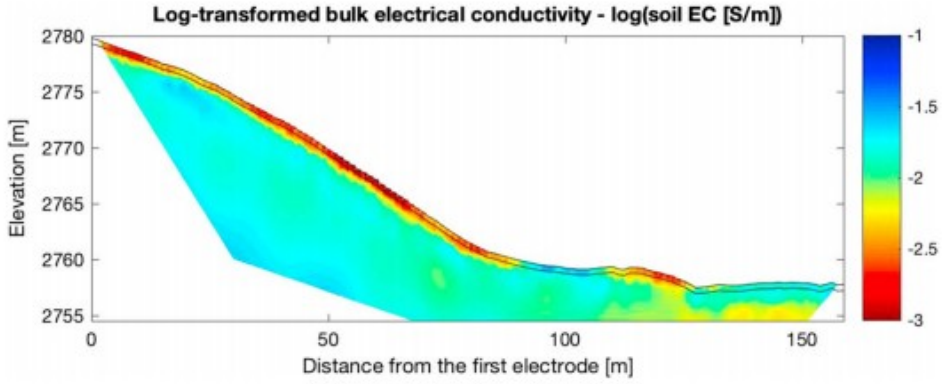

Figure 2. The figure shows the log (soil electrical conductivity [S/m]) obtained from an electrical resistivity tomography survey over a 158.75-m-long transect along the floodplain-hillslope topographical gradient. The black lines delineate the near-surface (0-50 cm) depth interval considered in our study.

The soil EC is generally influenced by subsurface properties such as water content, porosity, fluid EC, grain surface conductivity, soil cementation, and soil temperature (Archie, 1942; Friedman, 2005; Revil et al., 1998). In this study, we consider only the near-surface 0- to 0.5-m-depth interval, which is an important zone for plant-soil interactions. In environments where fluid EC (i.e., salinity) does not vary extensively (as is the case along this transect), the spatial variations in soil EC can be connected primarily to changes in soil moisture content (S. S. Hubbard et al., 2013) and soil characteristics (i.e., porosity, soil cementation, and grain surface conductivity, amount of clay in the soil). Since soil texture and soil moisture often covary, ERT can provide a spatially smoothed and “continuous” proxy for soil moisture compared to

direct, point-scale soil moisture measurements (Dafflon et al., 2017; Robinson et al., 2008). We also measured soil moisture along the transect using a soil-moisture-trase-system time domain reflectometer (TDR, 20-cm probe length) and performed a correlation analysis between the soil moisture and soil EC (Figure 3). The inferred correlation coefficient between soil EC and the soil moisture data was 0.69, suggesting that at this site, soil EC is significantly influenced by soil moisture. Because the volume sensed by the TDR is relatively superficial (top 20 cm) and measurements are spatially sparse, the TDR soil moisture data were not used for further analysis.

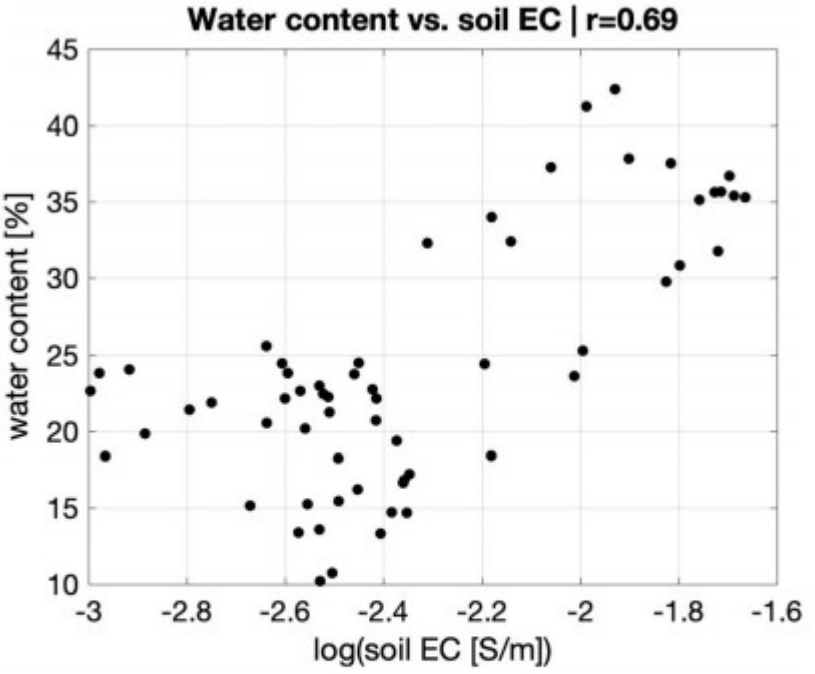

Figure 3. Soil electrical conductivity extracted from the top 40-cm depth in the electrical resistivity tomography versus the soil moisture content measured with a time domain reflectometer instrument. The behavior is due to the sensitivity of soil electrical conductivity to soil moisture content, while the limited fit is due to the fact that soil electrical conductivity is measured over a different volume and is also influenced by soil characteristics. Pearson's correlation is also reported.

2.2.4 Reference Data and Plant Community Distribution

We used a supervised machine-learning-based approach to estimate the plant community distribution. This method requires ground-truth information of the various communities, which is used to train the learning algorithm, validate the prediction, and ensure accuracy. Ground-truth data were collected using an real-time kinematic Differential Global Positioning Systems to accurately determine the spatial location of the different plant communities. The collected data were successively used to create spatial polygons as reference data for the supervised image classification. In our

analysis, we defined the following nine vegetation classes: deciduous forest, evergreen forest, riparian shrubland, sagebrush, shrubland, lupine meadow, veratrum, bunchgrass meadow, and forb. We also defined five nonvegetation classes: river, lake, man-made, bare area, and shadow. The vegetation classes were determined based on their spatial dominance and special characteristics. For example, sagebrush was distinguished from the more general shrubland classification because of its abundance across the hillslope. Veratrum has a unique structure with a tall canopy, presenting a quite homogeneous spatial coverage structure. Lupine, being a N-fixing plant, is important for nitrogen cycling (Myrold & Huss-Danell, 2003) and has been observed to be a dominant species in this lower montane floodplain-hillslope. Other vegetation classes, such as shrubland, bunchgrass meadow, and forb, presented a mixture of several species that together contributed to the particular class's spectral signature.

3 Methodology

To address our research hypothesis of coupled soil, topography, and plant variability, our methodology includes two components. First, we develop the high-resolution, remote-sensing, data-fusion framework, which enables us to delineate plant distribution at a sufficiently high resolution. Second, we present a statistical approach to quantify the high-resolution covariability between the plant communities, soil, and topographical properties to identify key controls of the plant community spatial distribution.

3.1 Image Classification for the Plant Community Mapping

We have developed a data-fusion framework that integrates multisource remotely sensed data to map plant communities over a floodplain-hillslope system (see scheme in Figure 4). Specifically, the goal is to estimate plant class at each pixel, based on multiple predictors (i.e., features) extracted from multispectral and LiDAR data. Although previous studies have mostly focused on single pixel information (Nijland et al., 2015; Roth et al., 2015), our framework takes into account the pixel spatial arrangement, which refers to the spatial relations between pixels and their neighborhood, such as shape characteristics, texture, and spatial coverage (Li et al., 2014) of the structures presented. In this approach, which is defined as spectral-spatial (Falco et al., 2015), each pixel has both direct data values—such as LiDAR-derived plant height or spectral reflectance—and other attributes from a contextual analysis. These predictors are then used as inputs to a supervised learning algorithm to predict plant communities' distributions and produce the final classification map.

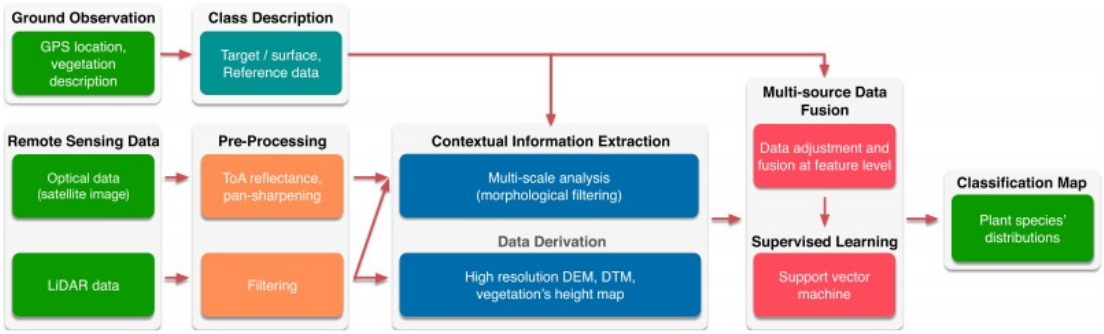

Figure 4. General scheme of the proposed data fusion framework for plant community mapping.

In this study, the contextual analysis is performed using a multilevel filtering procedure based on morphological operators (Matheron, 1975; Najman & Talbot, 2010; Serra, 1982; Soille, 2004) denoted as self-dual-attribute filters. These operators are defined as edge-preserving filters and are used to partition an image into spatially smooth regions (i.e., spatial clusters) according to a predefined homogeneity constraint. The extraction of spatially homogeneous regions minimizes the within-class spectral variability introduced by the high geometrical detail (Bruzzone & Demir, 2014), so that the classification map is less affected by “salt-and-pepper” noise.

We exploit these morphological operators within a recently developed analytical construct (Cavallaro et al., 2017) to perform an automatic multilevel contextual analysis by extracting spatial features (i.e., filtered images) at different scales to better characterize the different plant communities. (Here scale is the filter parameter and represents the number of pixels composing homogeneous regions.) The multiscale contextual analysis results in a stack of filtered images, one for each filtering step. The stack is denoted as a morphological self-dual attribute profile (SDAP), in which regions having similar properties at different scales are preserved or merged to their surroundings according to a set of scale parameters (similar to a hierarchical segmentation procedure). This strategy provides a way to capture large-scale spatial variability and local-scale trends in heterogeneity. (More details with graphical examples are reported in the supplemental material).

We performed the multiscale contextual analysis to build SDAPs for both the plant's height map and the multispectral data set. In the case of the height map, the procedure was applied directly to the map, identifying three thresholds and creating a stack of four images: the original map and a set of three images filtered using the three identified thresholds. Morphological operators are in general nonlinear transformations computed on an ordered set of values. Therefore, any extension to multivariate values is an ill-posed problem. In the case of the multispectral data set, which is composed of eight spectral bands, the direct application of morphological filtering is thus not possible. A common strategy is to apply the morphological operator to

each spectral band and stack the resulting filtered images together. However, this procedure would increase the dimensionality, with the resulting introduction of redundant information. In this work, we applied principal component analysis (PCA) to extract the first principal component, which accounts for most of the data's variance, and use it as input to the multiscale analysis. The obtained SDAP is composed of four images (an example of which is depicted in Figure S1 in the supporting information). A feature level fusion (Lahat et al., 2015) via image concatenation was then applied to the various stacks of images (i.e., the original spectral data set and the two SDAPs), whose combination gave an image vector composed of 16 images. Such a vector was then used as input into the machine-learning algorithm.

To perform the image classification, we used a support vector machine (SVM) classifier with a radial basis function kernel as a supervised learning algorithm. The algorithm is based on the LIBSVM (Chang & Lin, 2011) library developed for the MATLAB environment, using a one-against-one multiclass strategy. SVM has been commonly used in the remote-sensing-based land-cover classification. The algorithm requires the estimation of the regularization parameter, C, and the kernel parameter, gamma. We performed a cross validation based on a grid-search approach. Specifically, we considered exponentially growing sequences of C and gamma, with C = 10^{-2}, 10^{-1}, ... , 10^{4}, and gamma = 2^{-3}, 2^{-2}, ... , 2^{4}.

In our analysis, we considered 250 training samples randomly selected from each single class, with the remaining samples as the test set. Statistical analysis was then performed over a 20-fold cross-validation procedure, in which training and test sets were randomly selected and mutually exclusive. The performance of the algorithm was evaluated by computing the confusion matrix, which is a table that shows how well each plant community was predicted by the model. The table also provides information on possible errors of omission (false negative) and commission (false positive). In particular, from the confusion matrix we derived single-class accuracies, which provide information on how a single plant community has been predicted, and the overall accuracy, which is computed as the sum of the number of correctly classified values, divided by the total number of values. Such quantities are computed for each *n*-fold iteration, and therefore, we report here the average accuracies and relative standard deviations. The standard deviation would provide information on the stability of the model. We also computed the Cohen's Kappa coefficients, which provide a measure of overall classification quality, by comparing the agreement against the performance expected by chance. The possible values range from +1 (perfect agreement) to 0 (no agreement above that expected by chance) to -1 (complete disagreement).

3.2 Identifying Controls for Plant Community Distribution

We derived topographic metrics that are considered as proxies for hydrological processes, such as slope gradient, profile curvature, topographic position index (TPI), topographic wetness index (TWI; Gillin et al., 2015), and flow accumulation (FA; Tarboton, 1997). Slope gradient represents the degree of inclination of the surface, while the profile curvature provides information on how rapidly the slope changes, as well as convex or concave features of microtopography. TPI is defined as the deviation from the moving average of DEM (at the scale of 5 m), representing microtopography (de Reu et al., 2013; Weiss, 2001). In the case of positive TPI values, the sample is located on a ridge, whereas for negative values, the sample is located in a depression; for values close to zero, the sample location is within flat areas. FA represents for each cell the upslope drainage area computed as the number of cells that drain to it. Cells having low values of FA (meaning there are no other cells flowing to them) generally correspond to the pattern of ridges (Jenson & Domingue, 1988). TWI is an index computed as ln (FA/slope) and is based on the assumption that topography controls the spatial pattern of soil moisture (Beven & Kirkby, 1979; Schmidt & Persson, 2003).

High TWI values indicate areas with converging terrain, whereas low values indicate areas with steep, diverging terrain. As mentioned in Schmidt and Persson (2003), TWI is highly dependent on a main flow line that can only be one pixel wide. This implies that TWI assumes no water redistribution around a topographical low point. Moreover, TWI does not provide reliable values in a flat environment (such as in a floodplain) because of the many sinks and relatively flat ground (slow flow). In such conditions, TWI has to be considered as wetness that could be added to soil due to direct income of upstream water on a specific cell. These topographic metrics were computed by using the MATLAB TopoToolbox ver. 2.2 software (Schwanghart & Scherler, 2014). In addition, near-surface (0- to 0.5-m depth) soil EC were computed as described in section 2.2.3 along the ERT line.

We first investigated the contribution of each metric to the spatial distribution of each plant community through statistical graphical methods, including boxplots. We then explored their intercorrelations using biplots constructed through PCA. PCA is a method for dimensionality reduction and can be used to transform an original set of correlated variables into a set of uncorrelated ones, namely, principal components that are a linear combination of the original ones. The linear transformation identifies those components that maximize the variance of the original multivariate data. By selecting the components that account for most of the variance, it is possible to express the main information in a lower dimensional data space. Biplots of principal components have been widely exploited as an effective way to visualize correlations between observations and variables, graphically described as points and vectors (Greenacre, 2010). In our study, variables have different units; therefore, data values were scaled using the mean and variance prior to PCA.

Statistical analysis was computed over a larger portion of the floodplain-hillslope site (see Figure 1b). The area includes the ERT transect, which was exploited for the analysis of the soil EC and its relations with the plant community distribution.

4 Results

4.1 Estimation of Plant Community Distributions

The multisource data used in our analysis are displayed in Figure 1. Specifically, Figure 1b shows a true color RGB composition of the WV-2 multispectral pan-sharpened optical data. The image depicts those classes that have a strong color characterization, such as bare areas, forest, and veratrum. However, the classes related to different plant communities, such as bunchgrass and shrubland, are more difficult to differentiate. Figure 1d shows the DTM capturing microtopography. The DTM is used for computing several topographic metrics, and also for computing the plant height map (i.e., the DTM is subtracted from the digital surface model), which is shown in Figure 1e. The height map reveals a certain variability within the floodplain-hillslope system, allowing the identification of three main regions with similar characteristics:

1. Riparian area, characterized by tall shrubs, ranging between 0.5 and 2 m.
2. Forest area, with the presence of both deciduous and evergreen trees, ranging from 10 m to a maximum of 23 m.
3. Open area along the hillslope, characterized by meadow and shrubs, with a plant height ranging between a few centimeters and 1 m.

The estimated plant community classification, based on the proposed method, is shown in Figure 5. The plant classes, which were not evident on the RGB composition (Figure 1b), are well delineated by our data-fusion technique. The map reveals a strong heterogeneity in the plant community distribution, as well as a general spatial organization within this floodplain-hillslope subsystem. Veratrum is, for example, present at the toeslope near the riparian zones as well as above the outcrop area (summit of the hillslope, in slightly concave areas), where we expect groundwater seepage. Forbs and shrubs can be found at the backslope, that is, the upper part of the hillslope, while lupine is dominant in the footslope, representing the middle area of the hillslope.

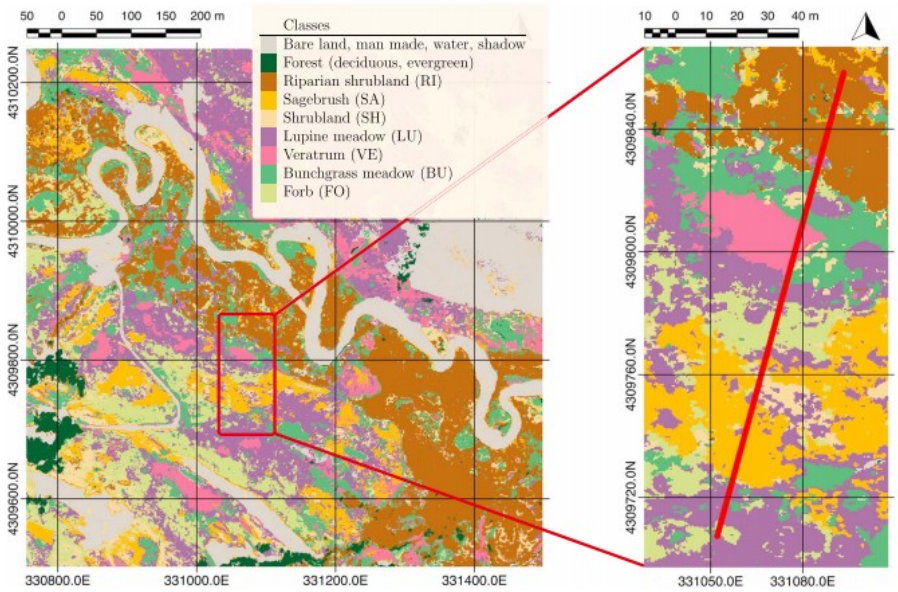

Figure 5. Classification map of the estimated plant community distributions. For visualization purposes, the classes that are not strictly related to the vegetation analysis, such as bare land, man-made, water, and shadow, are represented as a unique class (gray). The same concept is applied to the classes deciduous and evergreen forest, represented in dark green.

To quantify the performance of the new approach (which includes spectral, structural, and contextual information) relative to conventional methods for estimating plant types, we performed a validation experiment. We compared the performance of the proposed technique to those obtained by two standard strategies, in which the contextual information analysis was not included: (a) a classification approach that exploits spectral information only and (b) a classification approach that used both optical and LiDAR data. Table 1 shows class accuracies, overall accuracies, and kappa coefficients averaged over 20 folds, with relative standard deviations. The comparison quantitatively confirms the effectiveness of the proposed framework in accurately predicting the plant community distributions, showing the improvement when contextual analysis is included within the classification process. Fusing contextual, structural, and spectral information has significantly improved the delineation of vegetation classes. In the case of riparian shrubland, lupine meadow, shrubland, forb, and bunchgrass meadow, the new classification approach resulted in accuracies that are 14 percentage points (on average) higher than the standard approach. In order to test the statistical significance, we performed a *t* test between the result obtained with the standard method and the one obtained with the proposed framework. The *p* value resulted in $\ll 0.05$ (p value $\approx 1.7011e{-}30$), indicating that we can safely reject the null hypothesis (the null hypothesis that samples of the 20 folds for both classifications are extracted from the same distribution). The heat map depicted in Figure 6 represents the averaged confusion matrix over 20 folds obtained considering the proposed method. As previously mentioned, this metric provides a description of the classification performance for each single class, including the

misclassification error. Insights derived by this metric are discussed in-depth in Section 5.

Table 1
Performance of the Classification Strategies to Estimate Plant Community Distributions

Class *description*	Spectral	Spectral + LiDAR	Proposed data-fusion
Water river	95.66% (0.00)	95.87% (0.01)	*97.53%* (0.01)
Water lake	98.91% (0.00)	98.86% (0.00)	*99.09%* (0.01)
Man made	99.74% (0.00)	*99.91%* (0.00)	99.77% (0.00)
Bare area	97.50% (0.01)	97.89% (0.01)	*98.72%* (0.01)
Forest deciduous	*98.83%* (0.01)	97.07% (0.01)	97.02% (0.01)
Forest evergreen	*96.87%* (0.01)	96.39% (0.01)	96.51% (0.01)
Riparian shrubland	76.33% (0.01)	91.12% (0.01)	*94.26%* (0.01)
Sagebrush	91.73% (0.01)	92.60% (0.01)	*94.01%* (0.01)
Shrubland	70.82% (0.05)	78.01% (0.04)	*85.62%* (0.03)
Lupine meadow	62.92% (0.03)	63.02% (0.02)	*73.41%* (0.02)
Veratrum	92.99% (0.01)	92.70% (0.01)	*94.58%* (0.01)
Bunchgrass meadow	64.88% (0.02)	65.69% (0.03)	*79.33%* (0.02)
Forb	63.32% (0.02)	64.64% (0.02)	*78.29%* (0.01)
Shadow	*98.67%* (0.01)	98.21% (0.01)	98.14% (0.01)
OA	80.81% (0.01)	82.19% (0.01)	*87.98%* (0.01)
k	0.78 (0.01)	0.79 (0.01)	*0.85* (0.01)

Note. The table reports class accuracies, overall accuracies (OA) and Kappa coefficients (K), averaged over 20-fold, with relative standard deviations (in brackets). For each class, the best result among the three methods is reported in italics. Abbreviation: LiDAR light detection and ranging.

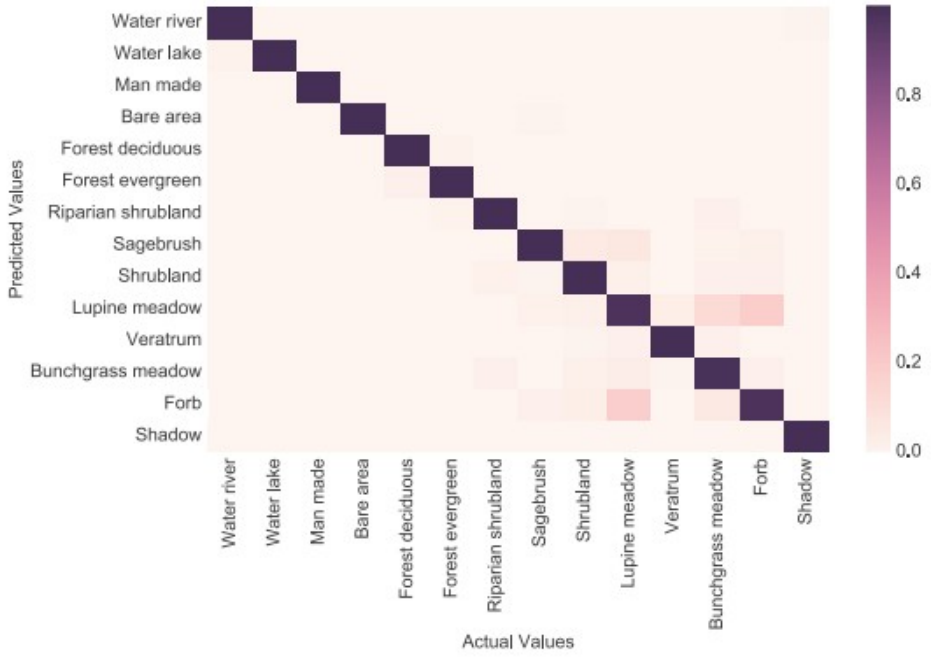

Figure 6. Heat map of the averaged confusion matrix over 20 folds obtained by applying the proposed method. The figure provides insight into the most common misclassified labels. For example, lupine meadow is sometimes classified as forb or bunchgrass meadow. Such misclassification error is due to the fact that lupine is nondominant species present in most of the meadow and forb areas, leading to mixed pixels. Therefore, the relative confusion between these communities is expected, as these classes indeed manifest similar spectral and structural characteristics, and their coverage boundaries are often not clearly defined, impacting the result of the classification.

4.2 Covariability of Plant Community, Soil Moisture, and Topographic Metrics

The relationships between the topographic metrics and plant communities over the floodplain-hillslope system (orange box in Figure 1b) are examined in Figure 7. The boxplot in Figure 7a shows in plant community as a function of slope, with the presence of nearly level (0.85°) to moderate steep areas (<30°; see Jahn et al., 2006, for slope categorization). The boxplot shows that sagebrush and forb are mainly located in high slope areas, while riparian shrubland and veratrum are located in low slope areas. Although the difference in curvature among the classes is minor (Figure 7b), sagebrush is found in relatively convex areas (e.g., small hills), while veratrum is located in concave areas (e.g., troughs).

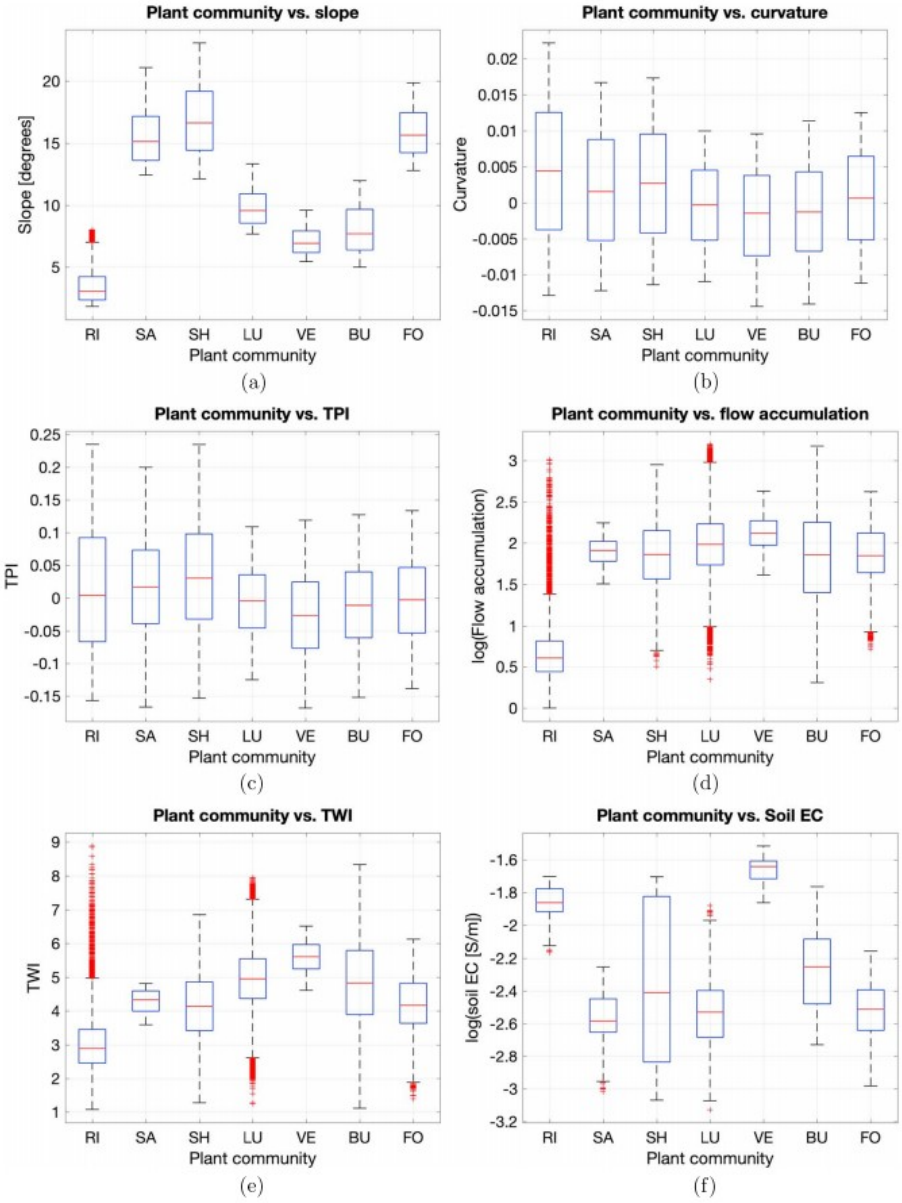

Figure 7. Analysis of co-variability over the floodplain-hillslope system between plant communities and (a) slope, (b) curvature, (c) topographic position index (TPI), (d) flow accumulation, and (e) topographic wetness index (TWI). (f) The result of the analysis of the soil electrical conductivity (EC) measured along the ERT transect. Plant legend: riparian shrubland (RI), sagebrush (SA), shrubland (SH), lupine meadow (LU), veratrum (VE), bunchgrass meadow (BU), and forb (FO).

In addition, the high TPI values (Figure 7c) correspond to the areas populated by sagebrush (indicating the presence of sagebrush in microtopographic hills), and low values with those populated by veratrum (indicating the presence of veratrum in microtopographic depressions). In terms of FA (Figure 7d), lupine, veratrum, and forb tend to grow in high FA areas. The TWI shown in Figure 7e provides observations similar to both curvature and TPI, such that sagebrush is located in areas characterized by low TWI, while veratrum is located in areas with high TWI. The boxplot in Figure 7f shows how the plant types vary with shallow soil EC computed along the ERT

transect. Soil EC is strongly influenced by lateral variations in soil moisture (Figure 3). Plant species such as veratrum and riparian shrubland are mostly associated with high soil EC (i.e., wetter soils), while sagebrush is associated with low soil EC.

The PCA-based biplot, shown in Figure 8, visualizes the covariability among the metrics, and clustering depending on the plant community types, computed along the ERT transect. The biplot is constructed by considering the first two principal components. The first component accounts for 39.6% of the total variance, while the second one accounts for 29.9%. The biplot shows that most plant communities have distinct clusters along two main gradients. The first gradient is described by the anticorrelated variables of soil EC and slope. Along this gradient, we can identify a series of clusters composed of sagebrush, forb, and lupine meadow, positively correlated with the slope and negatively correlated with soil EC. The second gradient, in direction of TWI and TPI, separates the clusters of veratrum and riparian shrubland, positively correlated with soil EC and negatively correlated with slope, and a third cluster composed of bunchgrass meadow located close to the center and tending toward more wet areas.

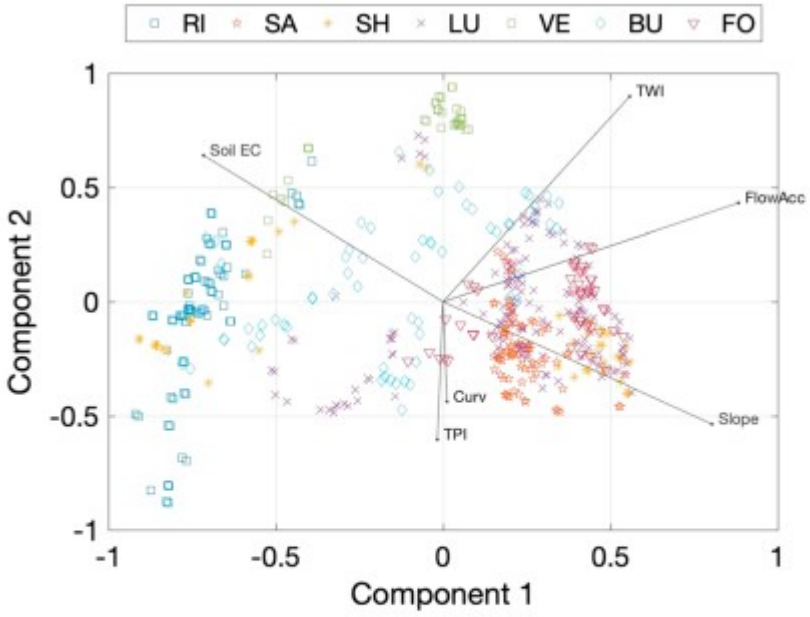

Figure 8. Biplot associated with the first and second principal components, where vectors represent the coefficients of the variables (metrics) and the points represent the scores of the observations. The length of each vector is proportional to the variance of each variable, while the angle between two vectors represents the correlation between the two variables. Plant legend: riparian shrubland (RI), sagebrush (SA), shrubland (SH), lupine meadow (LU), veratrum (VE), bunchgrass meadow (BU), and forb (FO).

The analysis reveals particular trends among different plants communities, especially for veratrum and sagebrush, whose spatial distributions are more localized with respect to the other communities. Veratrum grows in areas characterized by a quasi-flat terrain corresponding to areas located in depressions with high soil EC (negative TPI and high TWI). Similarly, riparian shrubland is located in quite flat areas with high soil EC and low slope. However, it is characterized by an alternating of depressions and ridges. On the other hand, sagebrush and forb seem to occupy similar areas characterized by a moderate slope and low soil EC, while sagebrush is spatially located along ridges or steep areas (positive TPI and low TWI).

5 Discussion

The proposed remote sensing data fusion framework obtained higher classification performance compared to both standard approaches and represents the first-time application for the meadow plants. Considering the classification results obtained by the two standard approaches, we notice that the use of the plant height map contributed to improving the estimation of several communities. In particular, the estimation of the riparian shrubland, which resulted in it being misclassified as deciduous forest, was improved by 15 percentage points. The class shrubland was improved by 7 percentage points. On the other hand, the presence of plant height brought a limited improvement to the more challenging meadow classes (lupine and bunchgrass meadows) and forbs, providing only a slightly higher predicting accuracy compared to the standard case. Including the spatial context can greatly improve the final estimation, increasing the prediction accuracy of shrubland (from 70.82% and 78.01% to 85.61%), lupine meadow (from 62.92% and 63.02% to 73.41%), bunchgrass meadow (from 64.88% and 65.69% to 79.33%), and forb (from 63.32% and 64.64% to 78.29%). In this case, the use of features that account for the spatial characterization between neighboring pixels allowed us to minimize the within-class spectral variability of the meadow communities, and at the same time, to better identify boundaries between them.

Despite this high performance, small misclassification errors were still present between the meadow classes. In particular, the confusion matrix depicted in Figure 6 shows that lupine meadow was sometimes classified as forb or bunchgrass meadow. Such misclassification error was due to lupine being present in most of the meadow and forb areas as a nondominant species, leading to mixed pixels. This in part results from the spatial resolution of 0.5 m not allowing for a single plant-signal recognition. Therefore, the relative confusion between these communities is expected, as these classes indeed manifest similar spectral and structural characteristics, and their coverage boundaries are often not clearly defined, slightly affecting the final estimation. Although their estimation represented a substantial challenge, the misclassification error was small compared to the error in the standard algorithms.

The use of high-resolution data allowed us to better observe the impact of microtopography on plant spatial coverage and diversity. Microtopography is known to play an important role in controlling the local hydrological patterns (Gillin et al., 2015; Moeslund et al., 2013; H. M. Wainwright et al., 2015), allowing plant communities to identify their own specific niche. In our analysis, microtopographic features were quantified in terms of slope, curvature, TWI, and TPI (Figures 7 and 9), which have shown the ability to differentiate depressions (which are often saturated with water during early growing season) from ridges (which are less moist). Such local features perturb soil moisture, soil type, nutrient cycling and availability (Duncan et al., 2013; Gillin et al., 2015), and water flow and drainage, with a direct impact on biological activity (Pei et al., 2010). By comparing the spatial aggregation of the plant communities from the community map (Figure 5) with the related TPI/TWI values, we can see that specific communities, and in some cases species, have a preferred microenvironment. Veratrum, for instance, is present in high-density patches located in depressions characterized by high soil moisture. Sagebrush is located on ridges or close to outcrop areas, which, in general, present a low soil-moisture concentration. The effect of microtopography can be observed also in the PCA-based biplot (Figure 8), where TWI, TPI, and curvature represent the second main environmental control. Differences in microtopography allow us to further characterize plant communities that grow in areas of similar soil moisture but different microtopography, such as veratrum and riparian shrubland, as well as sagebrush and forb.

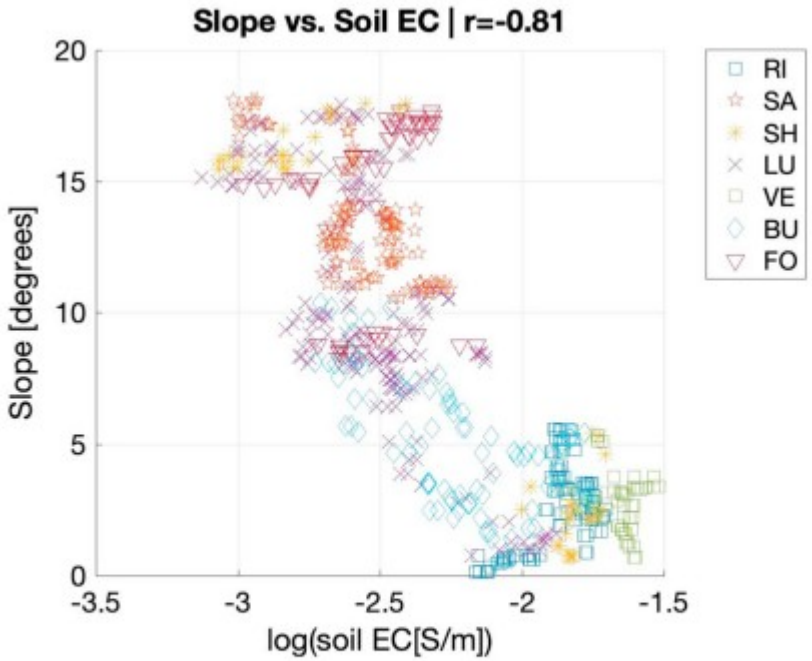

Figure 9. Relationship between the slope and soil electrical conductivity (EC). The scatterplot shows a strong Pearson's anticorrelation, indicating that slope could be used to inform on the soil properties within the hillslope system.

In addition, the strong anticorrelation between soil EC and slope observed in the multivariate PCA analysis was further investigated. Figure 9 shows a Pearson's correlation = -0.81 between the two metrics. This anticorrelation indicates that such topographic metrics could potentially be used to explain the spatial distribution of the plant communities and inform on the soil properties from the geophysical transect to a larger scale.

Envisioning such behavior, we further investigated the predictive capabilities of the topographic metrics and plant community map in estimating the soil EC along the ERT transect by using a random forest regression (Breiman, 2001). We defined training and test sets as nonoverlapping sets whose samples were randomly selected. The model produced a Pearson's correlation of 0.93 (Figure 10a). We investigated the predictive power of each variable and ranked them in terms of importance by permutating out-of-bag observations. The analysis identified the slope as the most important predictor, followed by the plant community distribution (PFT), and TPI (Figure 10b). We then extended the estimation of soil EC over the larger area (Figure 1b) by using the random forest model trained and validated along the ERT transect. The analysis, which is presented here in a qualitative form (Figure 10c), obtained results that are in line with those observed along the ERT transect. For instance, by comparing the estimated soil EC with the plant community map (Figure 5), areas with higher soil EC values are identified in the floodplain and in those areas populated mainly by veratrum. Low soil EC

values are estimated in those areas populated by sagebrush and forbs, characterized by a higher slope. These promising results are the starting point for our future investigations on the use of different proxies, such as topography and plant communities, to provide an extended estimation of the spatial variability of near-surface soil EC.

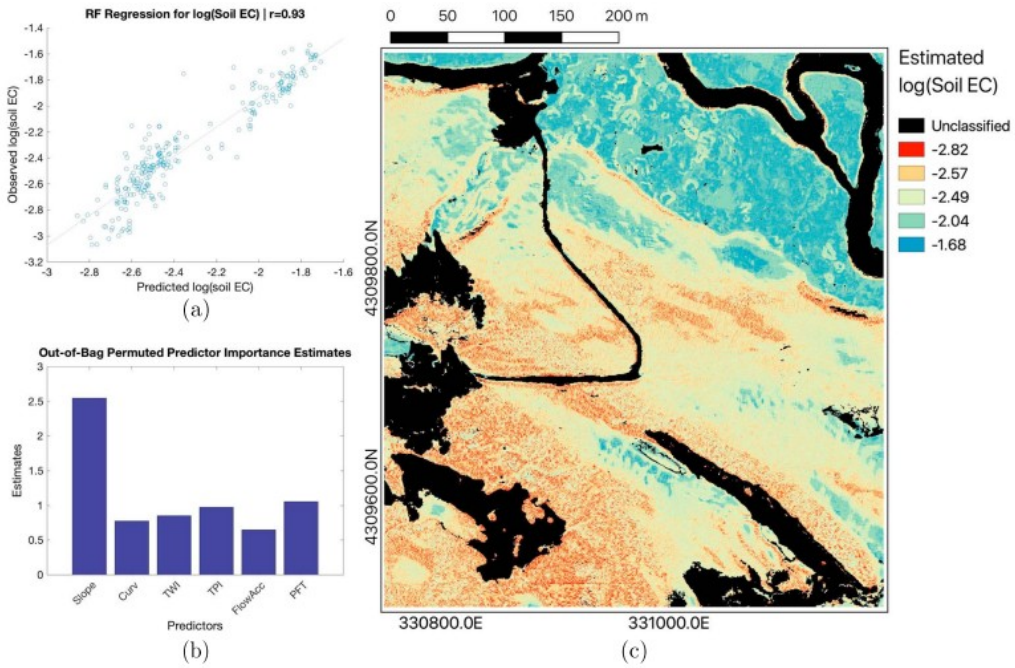

Figure 10. Prediction of log-transformed soil electrical conductivity (EC) by using a random forest regression. (a) Scatter plot between the observed and predicted soil EC along the electrical resistivity tomography (ERT) transect. The learning model is defined by training a subset (training set) of the available sample set along the ERT transect. The prediction is performed over a testing set. The training and testing sets are mutually exclusive (nonoverlapping) and composed by samples selected randomly. (b) The predictor importance shows that slope is the most important predictor, followed by the plant community distribution and topographic position index. (c) The map represents a qualitative prediction of soil EC over the extended study area. For the prediction, we exploit the regression model trained and validated over the ERT transect. The unclassified area corresponds to bare ground, forest, water, and shadow.

Given that soil moisture is the key control of spatial distribution, our results could provide insights on areas where plant-communities could be more susceptible to external disturbances within the hillslope. For example, increasing early snowmelt has been observed in this region, with a consequent reduction in soil moisture during the growing season (Sloat et al., 2015). Our results have shown that soil moisture is strongly varying along the hillslope and affected by the slope, suggesting that the physiological response of the different plant communities due to possible water limitation might not be spatially uniform but heterogeneous. Harte et al. (2015) have reported the transition from forbs to sagebrush, and we found that these two communities occupy a similar range in the topographic metrics and soil EC. This may suggest that forbs at this hillslope may be particularly susceptible to the shift. Previously, the modeling study by Pribulick et al. (2016) assumed a uniform change of the meadow to shrubs to predict the impact of climate change on ecohydrology. Therefore, it would be important to include a spatial metric that accounts for species susceptibility, which could be quite heterogeneous among the communities.

The proposed framework represents an improvement in the ability of our monitoring capabilities to provide high-resolution and spatially extensive information. The response to external perturbations can vary in both intensity and timing between plant communities. It is therefore of significant importance to characterize the spatial organization of plant communities when evaluating such heterogenous physiological behavior. Finally, the proposed framework can potentially be useful for long-term monitoring of meadow ecosystems. Understanding that functional groups can vary their response to plant encroachments, and that the nature of these interactions varies across environmental gradients (Kopp & Cleland, 2018), we can use accurate vegetation maps at high resolution to assess the local diversity and track the effect of plant encroachments—such as shifts and/or changes in community distribution due to disturbances such as early snowmelt and drought or associated with other perturbations (e.g., fire, logging). We also envision that this framework would serve as a bridge from plot-scale experiments to watershed-scale characterization without losing the natural spatial resolution at which interactions are observed. Additionally, the provided characterization could be used to guide sampling of soil biogeochemical investigations, which are sensitive to both plant community and soil properties.

6 Conclusion

In this study, we investigated the covariability among plant communities, soil EC, and several topographical metrics to assess the spatial organization of meadow plants along an intensive hillslope transect.

Results show that our framework estimated the spatial distribution of nine key plant communities with higher predictive accuracy (87% versus 80% overall; 85% versus 60% for shrubs) compared to conventional classification approaches. In particular, the inclusion of the contextual information allowed us to significantly improve the mapping of meadow plant communities—which are usually hard to separate because of their mixed spectral characteristics and/or similar structure. The joint use of high-resolution remote sensing (optical and LiDAR data) and geophysical measurements allowed us to characterize soil properties and land-surface variability at similarly resolution of 0.50 m, enabling the possibility to investigate the relationships between microtopography, soil properties, and plant spatial distribution at their native resolution.

Our analysis of the covariability showed that the heterogeneous plant community distribution is correlated with soil moisture, indicated by slope and soil EC data obtained from geophysical measurements, suggesting that soil moisture exerts a control on plant communities, which is consistent with previous studies at plot scale (Harte et al., 2015; Sloat et al., 2015). We observed the effect of microtopography on the spatial distribution of some of the plant communities. Microtopographic variability was measured in terms of curvature, TPI, and TWI, which are known to have a direct effect on soil

organic content (Pei et al., 2010), soil types (Gillin et al., 2015), and nutrients (Duncan et al., 2013) at local scale. Such metrics could explain the spatial distribution of particular plants communities located in areas with similar soil EC and slope but with different microtopographic reliefs. Along this line, the quantitative analysis of the estimation of soil EC along the ERT transect showed that slope is the most important predictor, followed by the plant community distribution and the microtopographic metrics (i.e., TPI, TWI, and curvature) in predicating soil EC values, producing a Pearson correlation of 0.93.

The classification and spatial covariance approach presented here demonstrates the potential of the proposed framework for effective integration of multisource data, including remote sensing and geophysical data, for accurately characterizing plant communities with high resolution and high fidelity. This highly transferable approach also allows the identification of potential interactions between subsurface and surface properties with plant communities. The high-fidelity estimates of plant community distribution can be an important means by which to populate high-resolution models seeking to describe water flows within vegetated systems, including variations in snow accumulation, runoff, evaporation (e.g., shading), and transpiration. With the increasing use of autonomous geophysical data and ease of collecting remote sensing information using various platforms, we expect that the developed approach will be transformational for monitoring plant dynamics in high resolution, and for revealing interactions between aboveground and belowground processes, from subsystem to entire watershed scales.

Acknowledgments

This material is based upon work supported as part of the Watershed Function Scientific Focus Area funded by the U.S. Department of Energy, Office of Science, Office of Biological and Environmental Research under award DE-AC02-05CH11231. The data sets used in this work, including the LiDAR, ERT, and derived products, can be found in Falco et al. (2019).

References

Allen-Diaz, B. H. (1991). Water table and plant species relationships in Sierra Nevada Meadows. *American Midland Naturalist*, 126(1), 30. https://doi.org/10.2307/2426147

Amundson, R., Heimsath, A., Owen, J., Yoo, K., & Dietrich, W. E. (2015). Hillslope soils and vegetation. *Geomorphology*, 234, 122– 132. https://doi.org/10.1016/j.geomorph.2014.12.031

Archie, G. E. (1942). The electrical resistivity log as an aid in determining some reservoir characteristics. *Transactions of AIME*, 146(01), 54– 62. https://doi.org/10.2118/942054-G

Benediktsson, J. A., Cavallaro, G., Falco, N., Hedhli, I., Krylov, V. A., Moser, G., Serpico, S. B., & Zerubia, J. (2018). Remote sensing data fusion: Markov models and mathematical morphology for multisensor, multiresolution, and multiscale image classification. In *Mathematical Models for Remote Sensing Image Processing* (pp. 277– 323). Cham, Switzerland: Springer International Publishing. https://doi.org/10.1007/978-3-319-66330-2_7

Beven, K. J., & Kirkby, M. J. (1979). A physically based, variable contributing area model of basin hydrology. *Hydrological Sciences Bulletin*, 24(1), 43– 69. https://doi.org/10.1080/02626667909491834

Binley, A., Hubbard, S. S., Huisman, J. a., Revil, A., Robinson, D. a., Singha, K., & Slater, L. D. (2015). The emergence of hydrogeophysics for improved understanding of subsurface processes over multiple scales. *Water Resources Research*, 51, 3837– 3866. https://doi.org/10.1002/2015WR017016

Breiman, L. (2001). Random Forests. *Machine Learning*, 45(1), 5– 32. https://doi.org/10.1023/A:1010933404324

Brown, T. B., Hultine, K. R., Steltzer, H., Denny, E. G., Denslow, M. W., Granados, J., Henderson, S., Moore, D., Nagai, S., SanClements, M., Sánchez-Azofeifa, A., Sonnentag, O., Tazik, D., & Richardson, A. D. (2016). Using phenocams to monitor our changing Earth: Toward a global phenocam network. *Frontiers in Ecology and the Environment*, 14(2), 84– 93. https://doi.org/10.1002/fee.1222

Bruzzone, L., & Demir, B. (2014). A review of modern approaches to classification of remote sensing data. In *Remote Sensing and Digital Image Processing* (pp. 127– 143). https://doi.org/10.1007/978-94-007-7969-3_9

Cavallaro, G., Falco, N., Dalla Mura, M., & Benediktsson, J. A. (2017). Automatic attribute profiles. *IEEE Transactions on Image Processing*, 26(4), 1859– 1872. https://doi.org/10.1109/TIP.2017.2664667

Chang, C.-C., & Lin, C.-J. (2011). LIBSVM: A Library for Support Vector Machines. *ACM Transactions on Intelligent Systems and Technology*, 2(3), 1–27. https://doi.org/10.1145/1961189.1961199

Collins, D. B. G., Bras, R. L., & Tucker, G. E. (2004). Modeling the effects of vegetation-erosion coupling on landscape evolution. *Journal of Geophysical Research*, 109, F03004. https://doi.org/10.1029/2003JF000028

Dafflon, B., Oktem, R., Peterson, J., Ulrich, C., Tran, A. P., Romanovsky, V., & Hubbard, S. S. (2017). Coincident above- and below-ground autonomous monitoring to quantify co-variability in permafrost, Soil and vegetation properties in Arctic tundra. *Journal of Geophysical Research: Biogeosciences*, 122, 1321– 1342. https://doi.org/10.1002/2016JG003724

Dalponte, M., Bruzzone, L., & Gianelle, D. (2012). Tree species classification in the Southern Alps based on the fusion of very high geometrical resolution

multispectral/hyperspectral images and LiDAR data. *Remote Sensing of Environment*, 123, 258– 270. https://doi.org/10.1016/j.rse.2012.03.013

de Reu, J., Bourgeois, J., Bats, M., Zwertvaegher, A., Gelorini, V., de Smedt, P., Chu, W., Antrop, M., de Maeyer, P., Finke, P., van Meirvenne, M., Verniers, J., & Crombé, P. (2013). Application of the topographic position index to heterogeneous landscapes. *Geomorphology*, 186, 39– 49. https://doi.org/10.1016/j.geomorph.2012.12.015

Dirnböck, T., Grabherr, G., Ginzler, C., Gottfried, M., & Dullinger, S. (2006). Mapping alpine vegetation based on image analysis, topographic variables and canonical correspondence analysis. *Applied Vegetation Science*, 6(1), 85. https://doi.org/10.1658/1402-2001(2003)006[0085:mavboi]2.0.co;2

Duncan, J. M., Groffman, P. M., & Band, L. E. (2013). Towards closing the watershed nitrogen budget: Spatial and temporal scaling of denitrification. *Journal of Geophysical Research: Biogeosciences*, 118, 1105– 1119. https://doi.org/10.1002/jgrg.20090

Ernakovich, J. G., Hopping, K. A., Berdanier, A. B., Simpson, R. T., Kachergis, E. J., Steltzer, H., & Wallenstein, M. D. (2014). Predicted responses of Arctic and alpine ecosystems to altered seasonality under climate change. *Global Change Biology*, 20(10), 3256– 3269. https://doi.org/10.1111/gcb.12568

Falco, N., Wainwright, H., Dafflon, B., Léger, E., Peterson, J., Steltzer, H., Wilmer, C., Rowland, J. C., Williams, K. H., & Hubbard, S. S. (2019). Remote sensing and geophysical characterization of a floodplain-hillslope system in the East River Watershed, Colorado. ESS-DIVE: Deep Insight for Earth Science Data. https://doi.org/10.21952/WTR/1490867

Falco, N., Benediktsson, J. A., & Bruzzone, L. (2015). Spectral and spatial classification of hyperspectral images based on ICA and reduced morphological attribute profiles. *IEEE Transactions on Geoscience and Remote Sensing*, 53(11), 6223– 6240. https://doi.org/10.1109/TGRS.2015.2436335

Franklin, J., Serra-Diaz, J. M., Syphard, A. D., & Regan, H. M. (2016). Global change and terrestrial plant community dynamics. *Proceedings of the National Academy of Sciences of the United States of America*, 113(14), 3725– 3734. https://doi.org/10.1073/pnas.1519911113

Friedman, S. P. (2005). Soil properties influencing apparent electrical conductivity: A review. *Computers and Electronics in Agriculture*, 46(1-3), 45– 70. https://doi.org/10.1016/j.compag.2004.11.001

Gillin, C. P., Bailey, S. W., McGuire, K. J., & Gannon, J. P. (2015). Mapping of hydropedologic spatial patterns in a steep headwater catchment. *Soil Science Society of America Journal*, 79(2), 440. https://doi.org/10.2136/sssaj2014.05.0189

Gonzalez, P., Asner, G. P., Battles, J. J., Lefsky, M. A., Waring, K. M., & Palace, M. (2010). Forest carbon densities and uncertainties from lidar, QuickBird,

and field measurements in California. *Remote Sensing of Environment*, 114(7), 1561– 1575. https://doi.org/10.1016/j.rse.2010.02.011

Govender, M., Govender, P. J., Weiersbye, I. M., Witkowski, E. T. F., & Ahmed, F. (2009). Review of commonly used remote sensing and ground-based technologies to measure plant water stress. *Water SA*, 35(5), 741– 752. https://doi.org/10.4314/wsa.v35i5.49201

Greenacre, M. J. (2010). *Biplots in practice*. Fundacion BBVA.

Hame, T., Mutanen, T., Rauste, Y., Antropov, O., Molinier, M., Quegan, S., Kantzas, E., Makela, A., Minunno, F., Benediktsson, J. A., Falco, N., Arnason, K., Storvold, R., Haarpaintner, J., Elsakov, V., & Rasinmaki, J. (2015). Enabling intelligent Copernicus services for carbon and water balance modeling of boreal forest ecosystems - North State. In *2015 IEEE International Geoscience and Remote Sensing Symposium (IGARSS)*, (Vol. 17, pp. 2048– 2051). Milan, Italy: IEEE. https://doi.org/10.1109/IGARSS.2015.7326203

Harte, J., Saleska, S. R., & Levy, C. (2015). Convergent ecosystem responses to 23-year ambient and manipulated warming link advancing snowmelt and shrub encroachment to transient and long-term climate-soil carbon feedback. *Global Change Biology*, 21(6), 2349– 2356. https://doi.org/10.1111/gcb.12831

Harte, J., Torn, M. S., Chang, F.-r., Feifarek, B., Kinzig, A. P., Shaw, R., & Shen, K. (1995). Global warming and soil microclimate: Results from a meadow-warming experiment. *Ecological Applications*, 5(1), 132– 150. https://doi.org/10.2307/1942058

Heideman, H. K. (2014). Lidar Base Specification (Ver. 1.2). October. https://doi.org/10.3133/tm11B4

Hinckley, E. L. S., Ebel, B. A., Barnes, R. T., Anderson, R. S., Williams, M. W., & Anderson, S. P. (2014). Aspect control of water movement on hillslopes near the rain-snow transition of the Colorado Front Range. *Hydrological Processes*, 28(1), 74– 85. https://doi.org/10.1002/hyp.9549

Hobbie, S. E. (2015). Plant species effects on nutrient cycling: Revisiting litter feedbacks. *Trends in Ecology & Evolution*, 30(6), 357– 363. https://doi.org/10.1016/j.tree.2015.03.015

Hoersch, B., Braun, G., & Schmidt, U. (2002). Relation between landform and vegetation in alpine regions of Wallis, Switzerland. A multiscale remote sensing and GIS approach. *Computers, Environment and Urban Systems*, 26(2–3), 113– 139. https://doi.org/10.1016/S0198-9715(01)00039-4

Hubbard, S. S., Gangodagamage, C., Dafflon, B., Wainwright, H., Peterson, J., Gusmeroli, A., Ulrich, C., Wu, Y., Wilson, C., Rowland, J., Tweedie, C., & Wullschleger, S. D. (2013). Quantifying and relating land-surface and subsurface variability in permafrost environments using LiDAR and surface geophysical datasets. *Hydrogeology Journal*, 21(1), 149– 169. https://doi.org/10.1007/s10040-012-0939-y

Hubbard, S. S., Williams, K. H., Agarwal, D., Banfield, J., Beller, H., Bouskill, N., Brodie, E., Carroll, R., Dafflon, B., Dwivedi, D., Falco, N., Faybishenko, B., Maxwell, R., Nico, P., Steefel, C., Steltzer, H., Tokunaga, T., Tran, P. A., Wainwright, H., & Varadharajan, C. (2018). The East River, Colorado, Watershed: A mountainous community testbed for improving predictive understanding of multiscale hydrological–biogeochemical dynamics. *Vadose Zone Journal*, 17(1), 1– 25. https://doi.org/10.2136/vzj2018.03.0061

Jahn, R., Blume, H. P., Asio, V. B., Spaargaren, O., & Schad, P. (2006). Guidelines for soil description. *Disease Management and Health Outcomes*, 1(4), 197– 209. https://doi.org/10.2165/00115677-199701040-00003

Jenson, S. K., & Domingue, J. O. (1988). Extracting topographic structure from digital elevation data for Geographic Information System analysis. *Photogrammetric Engineering and Remote Sensing*, 54(11), 1593– 1600.

Kopp, C. W., & Cleland, E. E. (2018). Plant community response to Artemisia rothrockii (Sagebrush) encroachment and removal along an arid elevational gradient. *Journal of Vegetation Science*, 29(5), 859– 866. https://doi.org/10.1111/jvs.12669

Laben, C. A, & Brower, B. V. (2000). Process for enhancing the spatial resolution of multispectral imagery using pan-sharpening. United States Patent 6 11: 875. https://doi.org/10.1074/JBC.274.42.30033.(51)

Lahat, D., Adali, T., & Jutten, C. (2015). Multimodal data fusion: An overview of methods, challenges, and prospects. *Proceedings of the IEEE*, 103(9), 1449– 1477. https://doi.org/10.1109/JPROC.2015.2460697

Li, M., Zang, S., Zhang, B., Li, S., & Wu, C. (2014). A review of remote sensing image classification techniques: The role of spatio-contextual information. *European Journal of Remote Sensing*, 47(1), 389– 411. https://doi.org/10.5721/EuJRS20144723

Markstrom, S. L., Hay, L. E., Ward-Garrison, C. D., Risley, J. C., Battaglin, W. A., Bjerklie, D. M., Chase, K. J., Christiansen, D. E., Dudley, R. W., Hunt, R. J., Koczot, K. M., Mastin, M. C., Regan, R. S., Viger, R. J., Vining, K. C., & Walker, J. F. (2012). Integrated watershed-scale response to climate change for selected basins across the United States. *U.S. Geological Survey Scientific Investigations Report 2011-5077*, 143.

Marston, R. A. (2010). Geomorphology and vegetation on hillslopes: Interactions, dependencies, and feedback loops. *Geomorphology*, 116(3–4), 206– 217. https://doi.org/10.1016/j.geomorph.2009.09.028

Matheron, G. (1975). *Random Sets and Integral Geometry*. New York: John Wiley.

Maxwell, R. M., & Condon, L. E. (2016). Connections between groundwater flow and transpiration partitioning. *Science*, 353(6297), 377– 380. https://doi.org/10.1126/science.aaf7891

Miller, C. R., Routh, P. S., Brosten, T. R., & Mcnamara, J. P. (2008). Application of time-lapse ERT imaging to watershed characterization. *Geophysics*, 73(3), G7– G17. https://doi.org/10.1190/1.2907156

Moeslund, J. E., Arge, L., Bøcher, P. K., Dalgaard, T., & Svenning, J. C. (2013). Topography as a driver of local terrestrial vascular plant diversity patterns. *Nordic Journal of Botany*, 31(2), 129– 144. https://doi.org/10.1111/j.1756-1051.2013.00082.x

Mountain Research Initiative EDW Working Group (2015). Elevation-dependent warming in mountain regions of the world. *Nature Climate Change*, 5(5), 424– 430. https://doi.org/10.1038/nclimate2563

Myrold, D. D., & Huss-Danell, K. (2003). Alder and lupine enhance nitrogen cycling in a degraded forest soil in Northern Sweden. *Plant and Soil*, 254(1), 47– 56. https://doi.org/10.1023/A:1024951115548

Najman, L., & Talbot, H. (2010). *Mathematical Morphology: From Theory to Applications*. Hoboken, NJ: ISTE-Wiley. https://doi.org/10.1002/9781118600788

Nijland, W., Coops, N. C., Nielsen, S. E., & Stenhouse, G. (2015). Integrating optical satellite data and airborne laser scanning in habitat classification for wildlife management. *International Journal of Applied Earth Observation and Geoinformation*, 38, 242– 250. https://doi.org/10.1016/j.jag.2014.12.004

Ohmura, A. (2012). Enhanced temperature variability in high-altitude climate change. *Theoretical and Applied Climatology*, 110(4), 499– 508. https://doi.org/10.1007/s00704-012-0687-x

Palace, M. W., Sullivan, F. B., Ducey, M. J., Treuhaft, R. N., Herrick, C., Shimbo, J. Z., & Mota-E-Silva, J. (2015). Estimating forest structure in a tropical forest using field measurements, a synthetic model and discrete return lidar data. *Remote Sensing of Environment*, 161, 1– 11. https://doi.org/10.1016/j.rse.2015.01.020

Paris, C., & Bruzzone, L. (2015). A three-dimensional model-based approach to the estimation of the tree top height by fusing low-density LiDAR data and very high resolution optical images. *IEEE Transactions on Geoscience and Remote Sensing*, 53(1), 467– 480. https://doi.org/10.1109/TGRS.2014.2324016

Pei, T., Qin, C.-Z., Zhu, A.-X., Yang, L., Luo, M., Li, B., & Zhou, C. (2010). Mapping soil organic matter using the topographic wetness index: A comparative study based on different flow-direction algorithms and kriging methods. *Ecological Indicators*, 10(3), 610– 619. https://doi.org/10.1016/j.ecolind.2009.10.005

Pelletier, J. D., Barron-Gafford, G. A., Gutiérrez-Jurado, H., Hinckley, E. L. S., Istanbulluoglu, E., McGuire, L. A., Niu, G. Y., Poulos, M. J., Rasmussen, C., Richardson, P., Swetnam, T. L., & Tucker, G. E. (2018). Which way do you lean? Using slope aspect variations to understand critical zone processes and

feedbacks. *Earth Surface Processes and Landforms*, 43(5), 1133– 1154. https://doi.org/10.1002/esp.4306

Pribulick, C. E., Foster, L. M., Bearup, L. A., Navarre-Sitchler, A. K., Williams, K. H., Carroll, R. W. H., & Maxwell, R. M. (2016). Contrasting the hydrologic response due to land cover and climate change in a mountain headwaters system. *Ecohydrology*, 9(8), 1431– 1438. https://doi.org/10.1002/eco.1779

Price, K. (2011). Effects of watershed topography, soils, land use, and climate on baseflow hydrology in humid regions: A review. *Progress in Physical Geography*, 35(4), 465– 492. https://doi.org/10.1177/0309133311402714

Rangwala, I., Sinsky, E., & Miller, J. R. (2013). Amplified Warming projections for high altitude regions of the Northern Hemisphere mid-latitudes from CMIP5 models. *Environmental Research Letters*, 8(2), 024040. https://doi.org/10.1088/1748-9326/8/2/024040

Revil, A., Cathles, L. M., Losh, S., & Nunn, J. A. (1998). Electrical conductivity in shaly sands with geophysical applications. *Journal of Geophysical Research*, 103, 23,925– 23,936. https://doi.org/10.1029/98JB02125

Robinson, D. A., Campbell, C. S., Hopmans, J. W., Hornbuckle, B. K., Jones, S. B., Knight, R., Ogden, F., Selker, J., & Wendroth, O. (2008). Soil moisture measurement for ecological and hydrological watershed-scale observatories: A review. *Vadose Zone Journal*, 7(1), 358. https://doi.org/10.2136/vzj2007.0143

Roth, K. L., Roberts, D. A., Dennison, P. E., Alonzo, M., Peterson, S. H., & Beland, M. (2015). Differentiating plant species within and across diverse ecosystems with imaging spectroscopy. *Remote Sensing of Environment*, 167, 135– 151. https://doi.org/10.1016/j.rse.2015.05.007

Rubin, Y., & Hubbard, S. S. (2005). *Hydrogeophysics*, 41. https://doi.org/10.1007/0-306-48065-4

Rücker, C., Güther, T., & Spitzer, K. (2006a). 3-D modeling and inversion of dc resistivity data incorporating topography—Part I: Modeling. *Geophysical Journal International*, 166(2), 495– 505. https://doi.org/10.1111/j.1365-246X.2006.03010.x

Rücker, C., Güther, T., & Spitzer, K. (2006b). 3-D modeling and inversion of DC resistivity data incorporating topography —Part II: Inversion. *Geophysical Journal International*, 166, 506– 517.

Rudolph, S., van der Kruk, J., von Hebel, C., Ali, M., Herbst, M., Montzka, C., Pätzold, S., Robinson, D. A., Vereecken, H., & Weihermüller, L. (2015). Linking satellite derived LAI patterns with subsoil heterogeneity using large-scale ground-based electromagnetic induction measurements. *Geoderma*, 241-242, 262– 271. https://doi.org/10.1016/j.geoderma.2014.11.015

Schmidt, F., & Persson, A. (2003). Comparison of DEM data capture and topographic wetness indices. *Precision Agriculture*, 4(2), 179– 192. https://doi.org/10.1023/A:1024509322709

Schwanghart, W., & Scherler, D. (2014). TopoToolbox 2 – MATLAB-based software for topographic analysis and modeling in Earth surface sciences. *Earth Surface Dynamics*, 2(1), 1– 7. https://doi.org/10.5194/esurf-2-1-2014

Serra, J. (1982). *Image Analysis and Mathematical Morphology*. London: Academic Press, Inc.

Sloat, L. L., Henderson, A. N., Lamanna, C., & Enquist, B. J. (2015). The effect of the foresummer drought on carbon exchange in subalpine meadows. *Ecosystems*, 18(3), 533– 545. https://doi.org/10.1007/s10021-015-9845-1

Soille, P. (2004). *Morphological Image Analysis. Principle and Applications*, (2nd Edion ed., Vol. 24, p. 11). Berlin, Heidelberg: Springer. https://doi.org/10.1007/978-3-662-05088-0

Spasojevic, M. J., Bowman, W. D., Humphries, H. C., Seastedt, T. R., & Suding, K. N. (2013). Changes in alpine vegetation over 21 years: Are patterns across a heterogeneous landscape consistent with predictions? *Ecosphere*, 4(9), art117. https://doi.org/10.1890/ES13-00133.1

Sullivan, F. B., Ducey, M. J., Orwig, D. A., Cook, B., & Palace, M. W. (2017). Comparison of lidar- and allometry-derived canopy height models in an eastern deciduous forest. *Forest Ecology and Management*, 406, 83– 94. https://doi.org/10.1016/j.foreco.2017.10.005

Tarboton, D. G. (1997). A new method for the determination of flow directions and upslope areas in grid digital elevation models. *Water Resources Research*, 33(2), 309– 319. https://doi.org/10.1029/96WR03137

Viviroli, D., Dürr, H. H., Messerli, B., Meybeck, M., & Weingartner, R. (2007). Mountains of the world, water towers for humanity: Typology, mapping, and global significance. *Water Resources Research*, 43, W07447. https://doi.org/10.1029/2006WR005653

von Hebel, C., Matveeva, M., Verweij, E., Rademske, P., Kaufmann, M. S., Brogi, C., Vereecken, H., Rascher, U., & van der Kruk, J. (2018). Understanding soil and plant interaction by combining ground-based quantitative electromagnetic induction and airborne hyperspectral Data. *Geophysical Research Letters*, 45, 7571– 7579. https://doi.org/10.1029/2018GL078658

Wainwright, H. M., Dafflon, B., Smith, L. J., Hahn, M. S., Curtis, J. B., Wu, Y., Ulrich, C., Peterson, J. E., Torn, M. S., & Hubbard, S. S. (2015). Identifying multiscale zonation and assessing the relative importance of polygon geomorphology on carbon fluxes in an arctic tundra ecosystem. *Journal of Geophysical Research: Biogeosciences*, 120, 788– 808. https://doi.org/10.1002/2014JG002799

Wainwright, H., & Williams, K. (2017). LiDAR collection in August 2015 over the East River Watershed, Colorado, USA. https://doi.org/10.21952/WTR/1412542

Wang, Q., Fan, X., & Wang, M. (2014). Recent warming amplification over high elevation regions across the globe. *Climate Dynamics*, 43(1–2), 87–101. https://doi.org/10.1007/s00382-013-1889-3

Webb, R. W., Fassnacht, S. R., & Gooseff, M. N. (2018). Hydrologic flow path development varies by aspect during spring snowmelt in complex subalpine terrain. *The Cryosphere*, 12(1), 287– 300. https://doi.org/10.5194/tc-12-287-2018

Weiss, A. (2001). Topographic position and landforms analysis. In ESRI User Conference, San Diego, CA. Vol. 200.

Yetemen, O., Istanbulluoglu, E., Flores-Cervantes, J. H., Vivoni, E. R., & Bras, R. L. (2015). Ecohydrologic role of solar radiation on landscape evolution. *Water Resources Research*, 51, 1127– 1157. https://doi.org/10.1002/2014WR016169

Zimmermann, N. E., Kienast, F., Häme, T., Mutanen, T., Rauste, E., Antropov, O., Molinier, M., Quegan, S., Kantzas, E., Mäkelä, A., Minunno, F., Benediktsson, J. A., Falco, N., Árnason, K., Storvold, R., Haarpaintner, J., Elsakov, V., & Rasinmäki, J. (1999). Predictive mapping of alpine grasslands in Switzerland: Species versus community approach. *Journal of Vegetation Science*, 10(4), 469– 482. Cham, Switzerland. https://doi.org/10.2307/3237182